Online Monitoring of Controlled Radical Polymerization: Nitroxide-Mediated Gradient Copolymerization

Emmanuel Mignard,[†] Thierry Leblanc,[†] Denis Bertin,[‡] Olivier Guerret,[§] and Wayne F. Reed*[,†]

Physics Department, Tulane University, New Orleans, Louisiana 70118; Chemistry Department, U. Marseille, France; and Atofina Corp., Lacq, France

Received October 21, 2003; Revised Manuscript Received November 14, 2003

ABSTRACT: A comprehensive characterization of the controlled radical copolymerization of styrene and *n*-butyl acrylate comonomers is obtained by using a recently introduced method termed automatic continuous online monitoring of polymerization reactions (ACOMP). By simultaneously monitoring and combining signals from a continuously diluted reactor stream, light scattering, viscosity, differential refractive index, and UV absorption were used, in a model-independent fashion, to follow the weight-average molecular weight M_w, weight-average intrinsic viscosity $[\eta]_w$, the concentrations of each comonomer, and hence also the evolution of the average instantaneous and cumulative compositions along the chains as comonomers were consumed. The "composition profile" along the chain will largely influence the copolymer properties, and it is suggested that gradient copolymers might also be termed "profiled copolymers", which then includes di- and multiblock polymers. Invoking the Mayo−Lewis model allowed sequence length averages and reactivity ratios to be computed. It is believed that the use of ACOMP with gradient copolymerization will lead to a better understanding of underlying kinetics and mechanisms and eventually lead to the ability to control the composition profile formation during the polymerization reaction.

Introduction

Controlled radical polymerization (CRP) involves different mechanisms such as reversible addition−fragmentation chain transfer (RAFT), atom transfer radical polymerization (ATRP), and nitroxide-mediated polymerization (NMP).[1−6] All of these synthetic pathways provide major control of the monomer insertion in the growing polymer chains. Indeed, all of them have in common a basic equilibrium between activated and deactivated species (respectively $P_n^{\bullet}$ and P_n−X) as depicted in Scheme 1.

In the presence of monomer M, only a small fraction (∼5%) of activated species can propagate until they are thermoreversibly deactivated by the mediated radical X. This means there is a repeated growth cycle for every chain, with a result similar to living ionic polymerization. This control allows a targeted molecular weight (up to 80−100 kg/mol) with narrow polydispersity index (near 1.1) to be obtained. Because of this, CRP has opened up a new route to the synthesis of well-defined macromolecules. Moreover, it is now possible to consider new polymeric architectures that were not imaginable or difficult to synthesize before. Among them, gradient copolymers seem to be promising materials due to the emergence of new bulk properties, which have only recently begun to be investigated.[7−10] Novel aspects include brush copolymers,[11] starlike gradient copolymer arms on an aluminum oxide core,[12] phase behavior,[13,14] and interfacial activity.[15]

Gradient copolymers are defined as copolymers of two or more monomers, whose composition profile varies along the chain, reflecting variation in monomer concentrations as conversion proceeds. Consequently, gradient copolymers blend the properties of two or more different homopolymers in a way that depends on the nature of the composition profile. In principle, the profile itself can be monotonic, have maxima and minima, be quasi-periodic, abrupt (e.g., a diblock), etc. In this work we define the composition profile to be the instantaneous fractional composition at each point along the chain. The "gradient", per se, is actually the derivative of the composition profile with respect to conversion and is of less immediate interest than the composition profile itself. In this sense "gradient copolymers" might more generally be termed "profiled copolymers".

Scheme 1. General Scheme for CRP

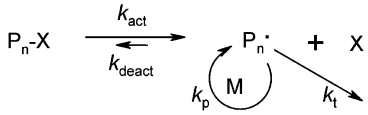

Currently, the characterization of gradient copolymers is difficult because traditional approaches, such as GPC and NMR, give only average cumulative values for a polymer population and cannot furnish the evolution of the instantaneous composition along the chain. Here, automatic continuous online monitoring of polymerization reactions (ACOMP) is adapted to provide the instantaneous composition (that is, the composition profile) as well as several other fundamental characteristics of gradient copolymers, while they are being formed.

Giz et al.[16] recently demonstrated ACOMP can be applied to free radical copolymerization reactions to obtain absolute, model-independent measurements of average composition and mass distributions, termed the copolymer "bivariate distribution" by Stockmayer[17] and others. Furthermore, by invoking models such as the Mayo−Lewis copolymer model,[18] it is also possible to

* Corresponding author.
† Tulane University.
‡ U. Marseille.
§ Atofina Corp.

10.1021/ma035589b CCC: $27.50
Published on Web 01/08/2004

Table 1. Experimental Conditions for Bulk and Solvent CRP Copolymerization Reactions

	volumes (mL)			mass (g)				
expt (st/ba %)	sty	BA	butyl acetate	SG1	MONAMS	*s*	target $DP_n^{(total)}$	target $M_n^{(total)}$
B1 (10/90)	50	450	0	0.064	2.628	0.014	566	70 904
B2 (20/80)	95	380	0	0.066	2.778	0.0045	520	63 799
B3 (30/70)	125	300	0	0.0442	1.946	0.0014	680	81 583
S0 (pure ba)	0	47	111	0.01	0.247	0.06	552	70 826
S1 (10/90)	4.6	42.5	111	0.01	0.248	0.06	564	70 775
S2 (30/70)	12.6	29.4	111	0.01	0.261	0.06	501	60 116
S3 (50/50)	19.3	19.7	111	0.01	0.23	0.06	552	63 497
S4 (70/30)	32.3	14.2	111	0.011	0.281	0.06	562	62 118

compute reactivity ratios and sequence length distributions.[16]

Here, we report the study of the nitroxide-mediated gradient copolymerization of styrene and *n*-butyl acrylate in bulk and in butyl acetate solution, with SG1[19,20] as the control agent and MONAMS[21−23] as the initiator. The goal of this work is to establish the means of obtaining comprehensive copolymer characterization in terms of cumulative and instantaneous composition (that is, composition profile), molecular mass, and intrinsic viscosity and to give examples of the data so obtained. This sets the stage for delving into the many kinetic and mechanistic aspects that the data reveal or that may be obtained by applying different models to the data.

Methods and Materials

The general ACOMP method, as first introduced by Florenzano et al.,[24] was used, but two different and improved extraction/dilution schemes have been substituted for the original one. In brief, the ACOMP method involves continuously extracting a small stream of fluid from the reactor and diluting it into the regime where the scattering and other detected properties are dominated by single polymer chains and not their interactions. This dilute stream is continuously fed through the desired combination of detectors and can be sampled as frequently as desired. The delay time between withdrawal and detection is strictly a function of tubing volumes and pump speeds and ranges typically from 2 to 20 min.

In this work two different extraction/dilution schemes were used. The first was the high-pressure, dual isocratic pump method first introduced by Chauvin et al.[25] Its advantages are that it provides exceptional stability for reactor extraction, has a small dead time (about 5 min), and is relatively inexpensive and simple to operate. Its biggest disadvantage is that it only works up to reaction viscosities of several hundred centipoise (cP). Here it was used only for reactions involving solvent and comonomers in the reactor, which took place at 120 °C. Butyl acetate was used for these experiments.

To investigate reactions in bulk monomer, where viscosities become quite high, a scheme was also developed using a gear pump for reactor extraction and utilizing combined low- and high-pressure mixing. This system is much more complex than the one just described but allows reactor viscosities of over 100 000 cP to be measured. Bulk reactions in this system were performed first, and THF was used as the dilution solvent.

The detector train comprised a prototype of the Brookhaven Instruments Corp. (Holtsville, NY) seven angle light scattering instrument, the BI-MwA, a home-built single capillary viscometer previously described in detail,[26] a Waters 410 differential refractometer, and a Shimadzu 10-AV VP, which outputs data for two different UV wavelengths. The reactor temperature was monitored via a K-type thermocouple. All of the instrument outputs were led through a 12 bit A/D converter (Data Translation 2801) to a computer. Data gathering and analysis software were written in house.

Gel permeation chromatography (GPC) for manually withdrawn reaction aliquots and end products was carried out on the same detector train as the ACOMP system. Instead of connecting the detector train to the diluted feed from the reactor, a GPC column (Polymer Labs 10 μm Mixed B) and an injector with a 0.1 mL loop were installed. Analysis software was previously written and modified to fit the format of the ACOMP detector train.

Dynamic light scattering measurements were made using a Brookhaven Instruments Corp. 90 Plus system. This instrument uses a 660 nm vertically polarized diode laser and 90° detection of scattered light. Analyses in terms of cumulants[27] of the autocorrelation function were obtained, and the average cumulant value allowed computation of the hydrodynamic radius, where $\eta = 0.007\,37$ P at 298 K was used for butyl acetate.

Butyl acrylate (BA, 99%), styrene (sty, 99%), and butyl acetate (99%) were used as received from Aldrich. The mediated radical, *N*-*tert*-butyl-1-diethylphosphono-2,2-dimethylpropyl nitroxide, SG1 (89%), and the alkoxyamine, methyl propionate-SG1 (MONAMS, 91%), were perfected and provided by Atofina Chemicals and used without any further purification. All amounts of reagent used are indicated in Table 1.

CRP reactions in solution were carried out according to the following ACOMP procedure: styrene, butyl acrylate, and butyl acetate were mixed together for several minutes at room temperature in a sealed flask. Then, 140 mL of the solution was poured in a three-necked flask equipped with a condenser, a nitrogen purge, and a thermometer probe. This solution was mixed and purged by nitrogen for at least 30 min in the reactor at room temperature. Before beginning the polymerization reaction, the ACOMP dilution solvent (butyl acetate) was pumped at 2 mL/min through the detector train to obtain the baseline of each instrument. Then, a continuous, low volume flow of the solution of monomers was withdrawn from the reactor (typically 0.12 mL/min) and mixed with a much higher volume flow of pure solvent (1.88 mL/min of butyl acetate) for 50 min. During the acquisition of the monomer baselines, an initiator mixture, consisting of MONAMS and the free SG1 diluted in 6 mL of an excess of the monomer solution, was prepared separately. This amount of monomer solution corresponds to the amount of reaction solution withdrawn from the reactor during the monomer baseline acquisition period of 50 min. This diluted initiator mixture was purged by nitrogen during at least 5−10 min at room temperature. Prior to the injection of the diluted initiator mixture, the reactor was gently heated to 115 °C to decrease the time necessary to reach the polymerization temperature. To start the polymerization, the diluted initiator mixture was quickly added with a gastight syringe through a septum, and the reactor was quickly heated to its final temperature, 120 °C.

Typical CRP reactions in bulk were carried out in a 600 mL jacketed filter reactor from Ace Glass Inc., equipped with a circulating oil bath (VWR Scientific), a mechanical stirrer (Caframo), a condenser, a nitrogen purge, and a thermometer probe. Because of the high viscosity of this kind of polymerization technique, the high viscosity, coupled low- and high-pressure mixing scheme mentioned above was used. A mixture of the total amount of monomers and the initiator system (MONAMS + free SG1) was stirred and purged under a nitrogen flow in a sealed flask at least 1 h prior to use. Then, this homogeneous mixture was poured into the reactor and immediately mixed under nitrogen pressure. When the detector baselines were stable, this reaction mixture was heated to 120 °C to start the polymerization reaction. In all ACOMP

Table 2. Properties of Monomers and Homopolymers in Butyl Acetate and in THF[a]

	$\partial n/\partial c$	rel absorp 266 nm	rel absorp 282 nm	ρ (g/cm^3)	mol mass (g/mol)
		Properties in Butyl Acetate			
sty	0.171	1	1	0.909	104.15
PS	0.206	0.084	≪0.01	1.04	NA[b]
BA	0.028	0.014	≪0.01	0.894	128.17
PBA	0.084	≪0.01	≪0.01	1.087	NA
		Properties in THF			
sty	0.164	1	NA	0.909	104.15
PS	0.198	0.056	NA	1.04	NA[b]
BA	0.016	0.011	NA	0.894	128.17
PBA	0.084	≪0.01	NA	1.087	NA

[a] Compared to styrene; for butyl acetate, $n = 1.3940$ and $\rho = 0.882$ g/cm^3. [b] NA = not applicable.

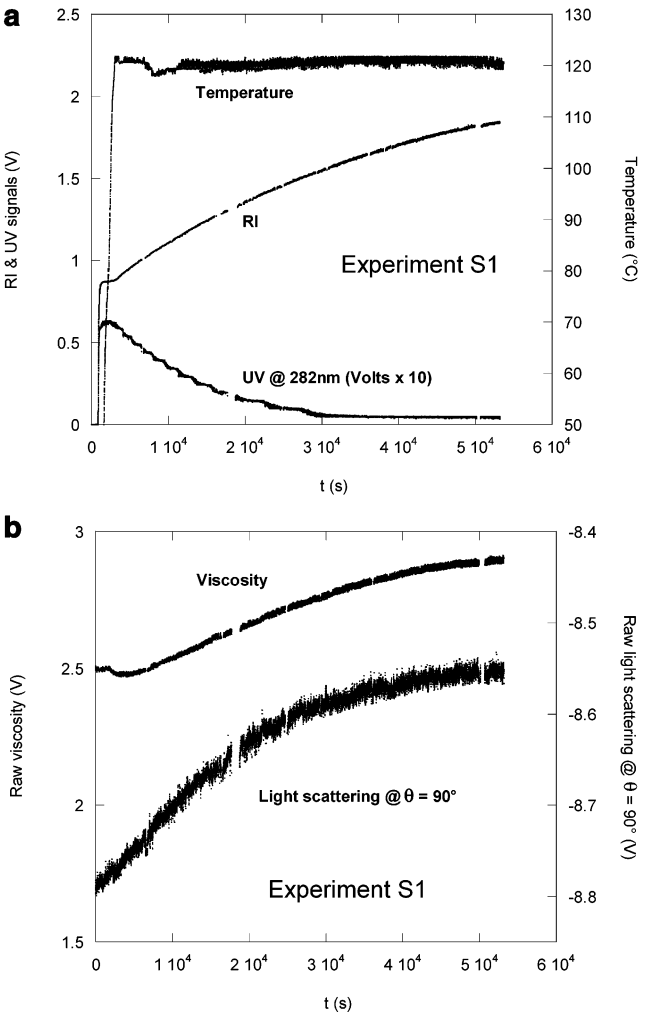

Figure 1. (a) Raw RI and UV (282 nm) data, and reactor temperature, for experiment S1. (b) Raw data for light scattering at 90° and viscosity for experiment S1.

experiments the temperature of the withdrawn reaction solution was quickly decreased to room temperature as soon as it left the reactor to avoid any polymerization reaction in the tubing.

Table 2 gives a summary of optical and other properties of styrene, BA, and their corresponding homopolymers. Table 1 provides a list of various bulk and solution reactions.

Figure 1a is an example of raw data gathered in an ACOMP gradient copolymerization reaction (experiment S1 in Table 1). The UV was set to 282 nm, at which only styrene absorbs measurably. Hence, the decrease of the UV directly measures styrene conversion. Because $\partial n/\partial c$ for both homopolymers is greater than that of the corresponding monomer, the RI signal increases as copolymerization proceeds. The temperature trace, provided by the reactor thermocouple, gave a temperature of 120.7 ± 0.7 °C during the reaction. The temperature signal has no delay and so is recorded in the figure 5 min before the ACOMP signals. Figure 1b shows raw data for viscosity and 90° light scattering from the same reaction. Both these signals increase as polymerization proceeds, and the molecular weight of the growing chains increases.

Results and Discussion

Determination of Comonomer Concentration and the Copolymer Composition Profile. There are four concentrations of relevance in the reactor: the concentration of comonomer A, c_{mA}, that of comonomer B, c_{mB}, the concentration of A in polymeric form c_{pA}, and that of comonomer B in polymeric form, c_{pB}. This requires four equations, two of which are supplied by conservation of mass. For the sty/BA comonomers, two other signals are available for the remaining two equations: UV absorption ($\lambda = 266$ nm and $\lambda = 282$ nm were used) and the RI signal.

In this work mass concentrations (g/cm^3) are denoted by c_{mA}, c_{pA}, etc., whereas the corresponding molar concentrations are represented by [A], [pA], etc., where [pA] is the molar concentration of A in polymeric form. These are related by $[A] = c_{mA}/m_A$ and $[pA] = c_{pA}/m_A$, where m_A is the molar mass of monomer A. In this work A = styrene and B = butyl Acrylate. When A (B) is used directly in an equation, this refers to moles of A (or B). When pA (or pB) is used in equations, it refers to the number of moles of A (or B) in polymeric form.

The values of $\partial n/\partial c$ for each monomer and corresponding polymer were determined by separate homopolymerization reactions according to the method of Brousseau et al.[28] and are summarized in Table 2 for both THF and butyl acetate.

The four concentrations were determined using the current ACOMP system according to the voltage response of the UV, V_{UV}, in conjunction with the RI voltage response, V_{RI}. Experiments were performed in the regime where the UV responded linearly to changes in absorbance, so that

$$V_{UV} = s(a_{sty}c_{mA} + a_{BA}c_{mB} + a_{PS}c_{pA}) \qquad (1)$$

where s is the volume fraction of reactor fluid present in the diluted solution flowing through the detector trains, and a_{sty}, a_{BA}, and a_{PS} are the coefficients appropriate for styrene, BA, and polystyrene (PS) and are directly related to the extinction coefficients, the UV cell path length (0.1 mm), and the UV output scale (4 AU/V). The ratios of these values are given in Table 2. Poly(butyl acrylate) (PBA) showed negligible absorption at the wavelengths used. V_{RI} is related to the concentrations in the reactor by

$$V_{RI} = s\left(\frac{\partial n}{\partial c_{mA}}c_{mA} + \frac{\partial n}{\partial c_{pA}}c_{pA} + \frac{\partial n}{\partial c_{mB}}c_{mB} + \frac{\partial n}{\partial c_{pB}}c_{pB}\right)\frac{dV_{RI}}{dn} \qquad (2)$$

where dV_{RI}/dn is the refractometer response factor. Before conversion begins $c_{mA} = c_{mA,0}$ and $c_{mB} = c_{mB,0}$, where the initial concentrations in the reactor $c_{mA,0}$ and $c_{mB,0}$ are known. Hence, s can be determined and cross-checked with the nominal value, determined by the relative pumping rates from the reactor and dilution sides of the automatic continuous mixing (ACM) system. In practice, before conversion begins, eq 2 is used to

determine the concentrations of A and B in the detector stream since $c_{mA,0}/c_{mB,0}$ in the reactor is known, along with the values of $\partial n/\partial c$ of each component. This yields a cross-check on the fractional flow from the reactor, s, which was always found to be within 2% of the nominal value. Values of s for each reaction are given in Table 1.

Whereas the concentrations in the detector streams are used directly for computation of M_w and $[\eta]_w$, as discussed below, the composition profile and related information are best expressed in terms of fractional molar conversion of each monomer, p_A and p_B, respectively, and in terms of total fractional molar conversion, p. Since the densities of the monomers and corresponding polymeric forms are different, density corrections must be made. If V_0 is the original volume of fluid in the reactor, including all monomer and solvent, and V is the volume at any time later, then the fractional molar conversion of A is given by

$$p_A = \frac{V[\mathrm{pA}]}{V_0[\mathrm{A}]_0} \tag{3}$$

and the total fractional molar conversion is

$$p = \frac{V}{V_0}\left(\frac{[\mathrm{pA}] + [\mathrm{pB}]}{[\mathrm{A}]_0 + [\mathrm{B}]_0}\right) \tag{4}$$

where V_0 is the initial volume of reactor fluid, and the volume V at any moment is

$$V = V_s(1 + R_A(1 - \delta_A p_A) + R_B(1 - \delta_B p_B)) \tag{5}$$

Here V_s is the volume of solvent in the reactor, R_A is the ratio of initial volume of monomer A to V_s, R_B is the ratio of initial volume of B to V_s, and

$$\delta_A = 1 - \frac{\rho_{mA}}{\rho_{pA}} \tag{6}$$

and likewise for δ_B. The ratio V/V_0 that is needed to compute p_A, p_B, and p is hence

$$\frac{V}{V_0} = \frac{1 + R_A(1 - \delta_A p_A) + R_B(1 - \delta_B p_B)}{1 + R_A + R_B} \tag{7}$$

where it is assumed that ideal mixing occurs. This provides the relationship between [A] and [pA]

$$[\mathrm{pA}] = \frac{V_0[\mathrm{A}]_0}{V} - [\mathrm{A}] \tag{8}$$

After a considerable amount of algebra it is found that

$$p_A = \frac{(1 + R_A + R_B)\left(1 - \frac{[\mathrm{A}]}{[\mathrm{A}]_0}\right) + \delta_B R_B\left(\frac{[\mathrm{A}]}{[\mathrm{A}]_0} - \frac{[\mathrm{B}]}{[\mathrm{B}]_0}\right)}{(1 + R_A + R_B) - \delta_B R_B\frac{[\mathrm{B}]}{[\mathrm{B}]_0} - \delta_A R_A\frac{[\mathrm{A}]}{[\mathrm{A}]_0}} \tag{9}$$

The corresponding expression for p_B is found by interchanging B for A everywhere. From p_A and p_B it is then also possible to compute p via eqs 4 and 7. The mass balance equations relating [pA] and [A], via eq 8 above, and [pB] and [B] can then be used in conjunction with the two RI and UV equations to compute [A] and [B] at each instant. Hence, p_A, p_B, p, [A], [pA], [B], and [pB] can all be determined from the measurements made from the RI and UV.

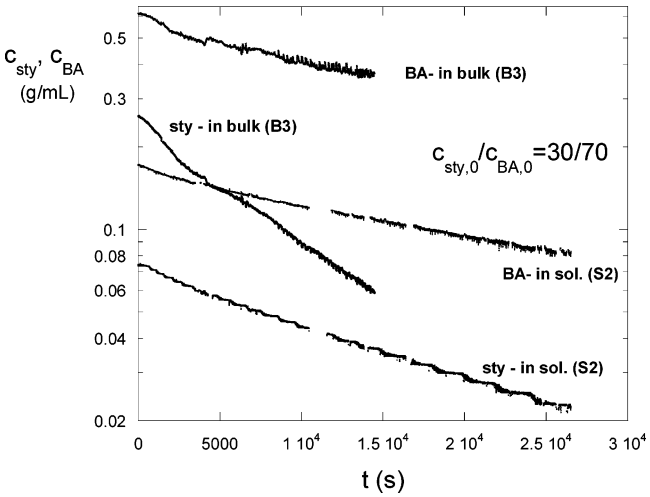

Figure 2. Concentration of sty and BA for identical ratios of sty/BA of 30/70 (g/g) and reaction conditions, except experiment B3 is in bulk, and S2 is at 30% comonomers by mass in butyl acetate.

Figure 2 shows the corresponding values of styrene and BA concentrations for experiments carried out with initial $c_{sty,0}/c_{BA,0} = 3/7$, corresponding to experiments S2 and B3 in Table 1, which refer to solution and bulk polymerization, respectively. Data of the type in Figure 2, and other variations, e.g. total molar monomer conversion vs time, should prove valuable in evaluating different mechanisms and kinetic models, such as have been amply treated theoretically.[29−32] Such work is separately in progress.

The type of concentration and conversion data shown in Figure 2 is extremely powerful and allows the computation of the average copolymer composition profile and an estimate of the reactivity ratios. Furthermore, it will be combined with the light scattering and viscosity data for M_w and $[\eta]$ analysis below.

The copolymer composition profile for component A can be defined as the instantaneous, fractional incorporation of A into the growing polymer chains, $F_{inst,A}$. This will cover any conceivable composition profile, and is never singular, since $F_{inst,A} \in [0,1]$. In the limiting case of a diblock, $F_{inst,A}$ can be discontinuous (but not singular) and resembles the Heaviside function. In mole terms A and B $F_{inst,A}$ is given

$$F_{inst,A} = \frac{\mathrm{d}A}{\mathrm{d}A + \mathrm{d}B} \cong \frac{\mathrm{d}[\mathrm{A}]}{\mathrm{d}([\mathrm{A}] + [\mathrm{B}])} \tag{10}$$

The approximation in terms of molar concentrations [A] and [B] instead of moles A and B is quite good, as can be seen by carrying through the total differentials dA and dB with the aid of eq 7, where d$A = V$ d[A] + [A] dV, and likewise for dB.

Because of the reactivity ratios and the changing concentrations of each comonomer $F_{inst,A}$ normally varies in the course of the reaction, so that the average local fraction of one comonomer at the start of the chain varies along the length of the chain. If $F_{inst,A}$ = constant throughout the reaction, this is equivalent to the azeotropic condition for free radical copolymerization, where there is no drift in the composition of the dead chains produced during the reaction. For the CRP case $F_{inst,A}$

= constant means that the average local concentration of the comonomers does not vary along the length of the chain.

The copolymer "gradient" itself is the derivative of $F_{\text{inst,A}}$ with respect to total conversion, that is, gradient = $\mathrm{d}F_{\text{inst,A}}/\mathrm{d}p$. While this quantity may be of interest for revealing how gradually or abruptly the composition profile changes, it is believed that the composition profile itself remains the primary characteristic of interest in determining the copolymer properties. It is noted that the gradient can be singular, for example at the junction between blocks in a block copolymer, unlike the composition profile whose value always lies between 0 and 1. In light of the greater importance of the composition profile vis à vis the gradient, it is suggested that gradient copolymers, in fact all copolymers with varying comonomer profiles, might also be termed "profiled copolymers".

The cumulative fractional composition of A in the growing chains $F_{\text{cum,A}}$ is defined as

$$F_{\text{cum,pA}} = \frac{pA}{pA + pB} = \frac{\int \mathrm{d[pA]}}{[\mathrm{pA}] + [\mathrm{pB}]} \tag{11}$$

where the use of molar concentrations is exact in this case. $F_{\text{inst,A}}$ is hence related to the $F_{\text{cum,A}}$ by

$$F_{\text{cum,pA}} = \frac{\int F_{\text{inst,pA}}\,\mathrm{d}p}{p} \tag{12}$$

where p is the total fractional conversion of both monomers, defined in eq 4, and $[\mathrm{A}]_0$ and $[\mathrm{B}]_0$ are the initial concentrations of A and B in the reactor Differentiation of eq 12 leads to

$$F_{\text{inst,A}} = F_{\text{cum,pA}} + p\,\frac{\mathrm{d}F_{\text{cum,pA}}}{\mathrm{d}p} \tag{13}$$

Because $F_{\text{inst,A}}$ involves the derivatives of data that inherently contain noise, there are several approaches to computing it. Different schemes were tried in this work: Taking derivatives directly from the data, point by point, is virtually meaningless, since the instantaneous slope from one point to the next, at the typical sampling speeds involved, produces almost random noise. The longer the sampling interval between data points, the less noisy the derivatives, so smoothing and numerical schemes are possible but not used here.

Another approach is to fit the monomer decay functions to given time-dependent functions [A](t) and [B](t), and then take the appropriate derivatives, analytically, for $F_{\text{inst,pA}}$ according to

$$F_{\text{inst,A}} = \frac{\mathrm{d[A]}/\mathrm{d}t}{\mathrm{d[A]}/\mathrm{d}t + \mathrm{d[B]}/\mathrm{d}t} \tag{14}$$

The problem here is to not introduce artifacts in $F_{\text{inst,A}}$ due to the fitting functions themselves. Higher-order polynomials (above third order), for example, tend to produce artificial ripples in $F_{\text{inst,A}}$.

The most promising approach so far, which avoids artifacts in the time fits, is to eliminate the time dependence completely by forming the sum [[A](t) + [B](t)] and plotting [A](t) vs the latter. Time then disappears and remains only as an optional parametrization for the domain and range. A fit of [A] = [A]([A] + [B]) is made, where [A] + [B] is the independent variable instead of time. The derivative of this function with respect to [A] + [B] then immediately yields the composition profile, $F_{\text{inst,A}}$. Because the functions remain parametrized in time, it is still possible to make graphs of $F_{\text{inst,A}}$ vs time as well as vs composition, total conversion, etc. In this work the fits are all possible with second-order polynomials, presumably partly because both comonomers respond simultaneously to factors that cause deviations from regularity in the time domain.

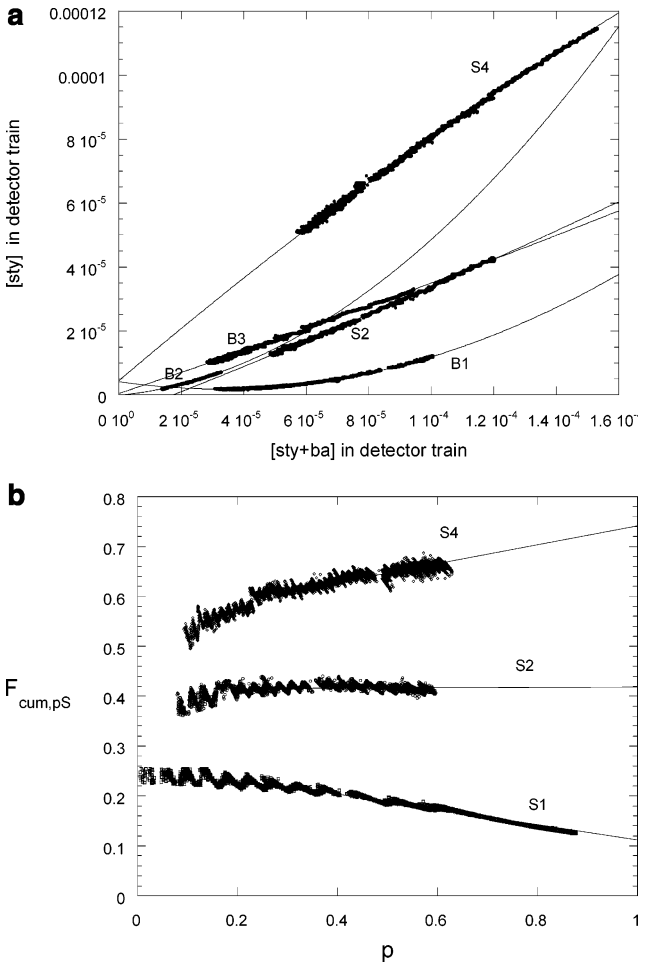

Figure 3. (a) Typical curves of [sty] vs [sty] + [BA], experiments B1−B3, S2, and S4, with second-order polynomial fits, according to eq 15. Fit parameters are shown in Table 3 for all experiments. (b) $F_{\text{cum,pS}}$ vs total molar conversion p for experiments S1, S2, and S4.

Figure 3a gives some examples of [sty] = [sty]([sty] + [BA]), used in subsequent determinations of $F_{\text{cum,pS}}$ and $F_{\text{inst,sty}}$, where

$$[\mathrm{sty}] = a_0 + a_1 x + a_2 x^2 \tag{15}$$

and x = ([sty] + [BA]). The associated quadratic fits to each curve are shown as well. These fits are traced out over the entire axis, for clarity, but only apply to the regime of concentrations in each case for which there are data points. $F_{\text{cum,pS}}$ is found directly by eq 11, from the values of [pS] and [pB] determined by the UV and RI detectors, and the mass balance equations. It is also possible to use the fitted forms of [sty], such as in Figure 3a, to have an analytical form of $F_{\text{cum,pS}}$.

In Figure 3b, $F_{\text{cum,pS}}$ is given directly from the detector-determined values of [sty] and [BA]. For the upper two curves data are absent below about 10%,

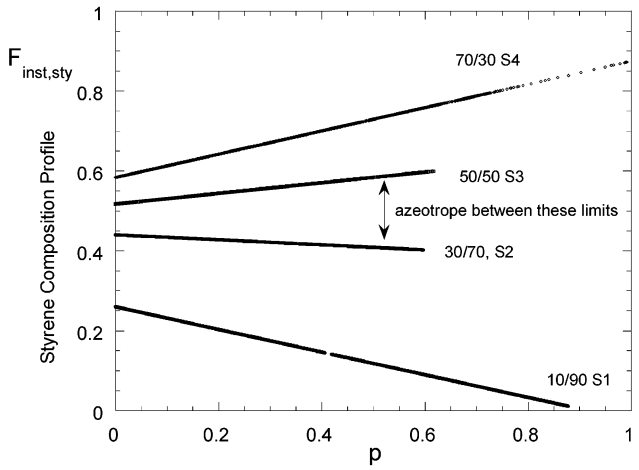

Figure 4. Styrene composition profile $F_{inst,sty}$, for experiments S1−S4, using the polynomial fit coefficients in Table 3.

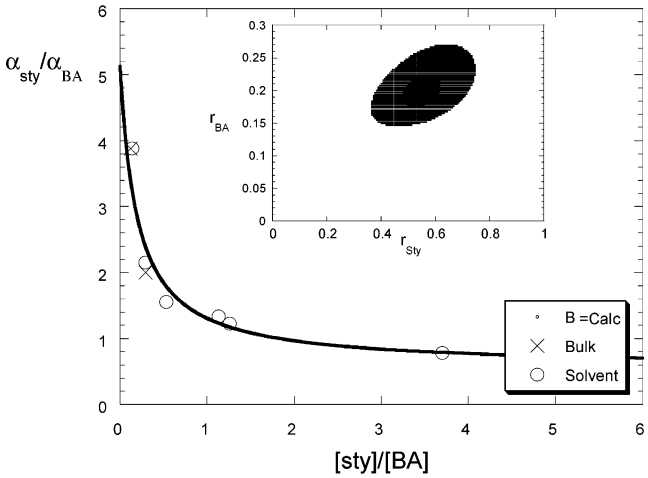

Figure 5. Ratio of styrene and BA rate constants vs [sty]/[BA], used in conjunction with eq 18 to determine the reactivity ratios. For both bulk and solvent experiments there is no measurable difference in the ratios. The inset shows the range of r_{sty} and r_{BA} values for rms errors of 4% (inner cluster of points) and 5% (larger cluster).

reflecting large uncertainties due to taking the ratio of small quantities of polymer. The extrapolations to $p = 1$ give the expected values for $F_{cum,pS}$ according to the initial ratio of [sty]/[BA].

Figure 4 shows the styrene composition profile, $F_{inst,sty} = a_1 + 2a_2x$, from the coefficients in eq 15, for several experiments in which the styrene/BA ratio was changed. The greatest fractional change (gradient) in the gradient occurs for the sty/BA 10/90 experiment. The azeotrope, for which $F_{inst,pS}$ is constant, should fall between the 50/50 and 30/70 limits. Integration of $F_{inst,pS}$ over $p = 0$ to 1 according to eq 12 yields the final molar fraction of f_{pS} at full conversion, which is equal to the initial mole fraction of sty, $f_{pS,0}$. The values of $F_{inst,sty}$ in the curves integrate to give values within a few percent of the initial mole fractions. At $p = 0$, $F_{inst,sty} = F_{cum,pS}$, which is seen to hold well when the $p = 0$ values in Figures 3b and 4 are compared. It is noted that the actual "gradient" of each of these linear composition profiles is constant.

One caveat regarding the composition profile is that, due to the on/off nature of CRP, all chains will reflect the average gradient obtained by ACOMP if the average dormant period between radical propagation periods is short compared to the time it takes for a significant change in comonomer concentrations.

Reactivity Ratios. The reactivity ratios r_A and r_B are defined as

$$r_A = \frac{k_{AA}}{k_{AB}}, \quad r_B = \frac{k_{BB}}{k_{BA}} \tag{16}$$

where k_{AA} is the rate constant for A adding to radical A* and k_{AB} is the rate constant for B adding to B*, etc.

Determination of the reactivity ratios using ACOMP was introduced in ref 16, in which both a complex numerical computer program was used to search optimum solutions in parameter space and a much simpler kinetic approach was taken. The agreement of the results for the sty/mma system between the two methods was excellent, so here only the kinetic method is used.

Referring to Figure 2, there are one or more straight line intervals of comonomer decay in each curve that can hence be approximated as quasi-first order decays over the intervals of the form

$$[A] = [A]_0 e^{-\alpha_A t} \quad \text{and} \quad [B] = [B]_0 e^{-\alpha_B t} \tag{17}$$

where $[A]_0$ and $[B]_0$ are the comonomer concentrations at the beginning of the interval considered quasi-first-order. The reactivity ratios can be determined by finding the ratio of these rate constants, using values of α_A, α_B, $[A]_0$, and $[B]_0$ both from individual and separate experiments, according to

$$\frac{\alpha_A}{\alpha_B} = \frac{1 + r_A\dfrac{[A]_0}{[B]_0}}{\dfrac{[A]_0}{[B]_0} + r_B} \tag{18}$$

The relative insensitivity of the right side of this equation to composition drift has been noted by Walling and Briggs,[33] and Kelen and Tudos have used this fact in developing their extended method.[34]

Figure 5 shows the results of this analysis. Points from both bulk reactions and in solvent (BuAc) are shown, and within the experimental uncertainties, there is no difference between bulk and solvent values. Significant differences in propagation rate constants for styrene and acrylates in different solvents have nevertheless been found.[35] The curve fit through the points in Figure 5 corresponds to the average values of r_A and r_B , discussed in the next paragraph.

The inset to Figure 5 was computed by forming a parameter space grid of pairs of discrete values for r_{sty} and r_{BA} and then computing the error in terms of the difference between experimental and theoretical points, divided by the experimental value for each point. The square root of the sum of the squares of this error for all points, divided by the number of points, gives the root-mean-square (rms) error. The cluster of points shows the region of the space that gives fractional rms errors of less than 5%, and the inner dark cluster is for rms errors less than 4%. From this, the best values are $r_{sty} = 0.55$ and $r_{BA} = 0.19$, for which the computed curve in Figure 5 is made. The range is $r_{sty} \in [0.39, 0.80]$ and $r_{BA} \in [0.15, 0.23]$. Although the best value of r_{sty} is low, the overall result compares reasonably to result results by Arehart and Matyjaszewski,[36] who also give a

compilation of reactivity ratios from different authors at different polymerization conditions, although it seems that any systematic temperature trend is masked by scatter in the data from report to report. Nevertheless, all reports agree that $r_{sty} > r_{BA}$, and the values range as $r_{sty} \in [0.60,1.2]$ and $r_{BA} \in [0.16, 0.29]$. As pointed out in ref 36, the scatter of values in the literature may be due more to the various methods and assumptions used in determining reactivity ratios[37] than to the different conditions under which the reactions were carried out. The fact that bulk and solvent values in this work are virtually identical supports this notion.

Sequence Length Considerations. The values of $F_{cum,pA}$ and $F_{inst,pA}$ determined above are model-independent and rely only on the detector signals and mass balance equations. The model-dependent notions of sequence length distributions (SLD) and averages from free radical polymerization can be translated to CRP. There are certain differences in interpretation, however. The sequence length averages of A (SLA), such as number-average $\langle N_A \rangle_n$ and weight-average $\langle N_A \rangle_w$ in free radical polymerization apply to all the chains propagating and then terminating over a short time interval around a given time. In the final population of dead chains, both the SLD and the average composition distribution change, according to what interval of conversion a specific chain was produced during. All chains produced in a given conversion interval have the same average composition ($F_{inst,pA}$) and SLD along the length of the entire chain; i.e., if segments from different parts of a chain are analyzed, the SLA of all the segments will be the same. The same holds for $F_{inst,pA}$.

In contrast, in CRP, since the chains live throughout the entire conversion, there is neither a unique $F_{inst,pA}$ nor SLA among different segments of a chain. Hence, although it is possible to otherwise directly use the model-dependent Mayo−Lewis expressions for SLD and SLA as in free radical copolymerization, these conceptual differences should be borne in mind.

The probability that A adds to radical A*, W_{AA}, is

$$W_{AA}(f_t) = \frac{r_A f_A(p)}{f_A(p)(r_A - 1) + 1} \tag{19}$$

where $f_A(p)$ is the mole fraction of A left in solution at conversion point p

$$f_A = \frac{[A]}{[A] + [B]} \tag{20}$$

The probability of having a sequence of k monomers in a row of type A, followed by a monomer B, $P_{A,k}$, then follows the well-known geometric distribution[38,39]

$$P_{A,k} = (1 - W_{AA}) W_{AA}^{\,k-1} \tag{21}$$

$P_{A,k}(p)$ from ACOMP measurements at each point p is hence the instantaneous sequence length distribution. The instantaneous number-average sequence length of monomer A, $\langle N_A \rangle_n$, is

$$\langle N_A \rangle_n(p) = \frac{1}{1 - W_{AA}(p)} \tag{22}$$

and the instantaneous weight-average sequence length of A, $\langle N_A \rangle_w$, is

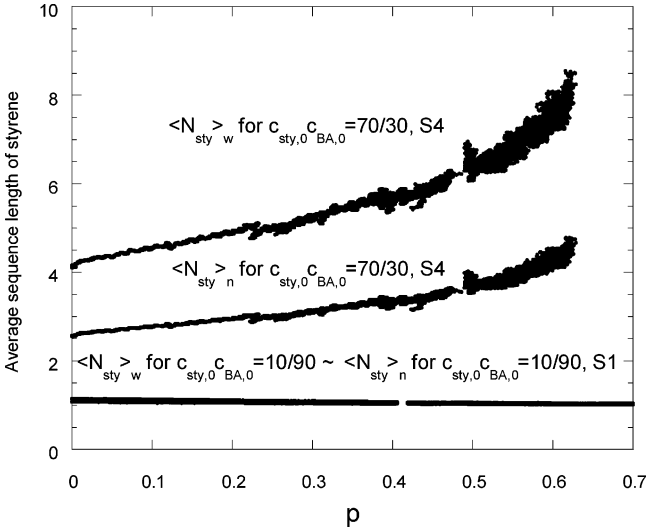

Figure 6. Number- and weight-average styrene sequence length distributions for experiments S1 and S4.

$$\langle N_A \rangle_w(p) = \frac{1 + W_{AA}(p)}{1 - W_{AA}(p)} \tag{23}$$

Cumulative values of the number and weight averages, $\langle N_A \rangle_{n,cumu}$ and $\langle N_A \rangle_{w,cumu}$, are

$$\langle N_A \rangle_{(w,n)cumu}(p) = \frac{\int_0^p \langle N_A \rangle_{(w,n)}(p')\, dp'}{p} \tag{24}$$

Figure 6 shows $\langle N_{sty} \rangle_n$ and $\langle N_{sty} \rangle_w$ vs total molar conversion for experiments S1 and S4. For the $c_{sty,0}/c_{BA,0}$ = 10/90 (S1) experiment there is so little styrene that both average sequence lengths are close to 1. In contrast, the 70/30 experiment shows that the sequence lengths start at 2.5 and 4, respectively, and effectively double by about 65% conversion, which reflects the higher local "blockiness" of styrene at the higher gradient values (see Figure 4).

Molecular Mass and Intrinsic Viscosity. Determining M_w for copolymers by light scattering has traditionally required measurements in three separate solvents because there are three distinct weight-average masses involved: the weight-average of A in polymeric form M_A, the weight-average of B in polymeric form M_B, and the total copolymeric M_w, this latter being the one usually sought. It was shown in ref 16 that the original light scattering equations for copolymers derived by Stockmayer et al.[40] and Bushuk and Benoit[41] could be manipulated and integrated such that M_w can be determined by ACOMP in a single solvent, during polymerization.

Fortunately, the light scattering equations for CRP gradient copolymerization are extraordinarily simpler than for the uncontrolled radical case. If the approximation is made that at any instant the width of the composition distribution is narrow compared to the average, since all propagating chains are "alive", then the only compositional heterogeneity at any point is the instantaneous width of the distribution, quite unlike the accumulated composition drift that occurs in uncontrolled radical polymerization, where dead chains of varying composition accumulate as the reaction proceeds. We can term this approximation that of "instantaneous compositional homogeneity", which then allows

the usual Zimm approximation to be used in the form given in refs 40 and 41

$$\frac{K'\nu^2 c_p}{I_R(q,c_p)} = \frac{1}{M_w}\left(1 + \frac{q^2\langle S^2\rangle_z}{3}\right) + 2A_2c_p + O(c_p^2) \qquad (25)$$

where $I_R(q,c_p)$ is the solvent subtracted absolute Rayleigh scattering ratio (cm^{-1}) from the copolymer solution of concentration c_p in the detector train. q is the usual scattering vector amplitude, $q = (4\pi n/\lambda)\sin(\theta/2)$, where n is the solvent index of refraction, λ the vacuum wavelength of the incident laser (677 nm), and θ is the angle in the scattering plane at which I_R is determined. K' is given for vertically polarized light by

$$K' = \frac{4\pi^2 n^2}{N_A\lambda^4} \qquad (26)$$

Equation 25 applies instantaneously, but ν, the weight-average differential refractive index increment, changes as the gradient copolymer composition changes according to

$$\nu = \frac{\partial n}{\partial(c_{pA} + c_{pB})} = y\frac{\partial n}{\partial c_{pA}} + (1-y)\frac{\partial n}{\partial c_{pB}} \qquad (27)$$

where

$$y = \frac{c_{pA}}{c_{pA} + c_{pB}} \qquad (28)$$

With values of M_w less than 100 kg/mol, the angular dependence of eq 25 could be ignored, and M_w values were determined by scattering at $\theta = 90°$.

Figure 7a shows M_w vs time for experiment S3, using the procedure outlined. Figure 7b shows M_w vs percentage of total monomer mass conversion for the same experiment. Also shown are the GPC values for M_w at different conversion points. These agree well with the continuous ACOMP values. The polydispersity index M_w/M_n did not change significantly during the course of this reaction and averaged 1.38 ± 0.2.

In the case of copolymerization it is often more convenient to deal in degree of polymerization when considering the initial stoichiometry and the expected mass. It is simple to show that the weight-average degree of polymerization N_w is related to M_w and $F_{cum,A}$, both experimentally available quantities, by

$$N_w = \frac{M_w}{(m_A - m_B)F_{cum,pA} + m_B} \qquad (29)$$

The target values for these are shown in Table 1.

Figure 7c shows M_w vs p for two other experiments, B2 and B3. The scales have been separated so that the data are not confused by overlap on the same graph. The salient features are that B2 has a nonzero intercept for M_w and shows some upward curvature, whereas B3 shows $M_w = 0$ at $p = 0$ and it has some downward curvature. Only in the ideal case of CRP where propagation is the predominant reaction, and in a small number of other limiting cases, will M_w be linear vs p. The actual shape of M_w vs p can vary widely on the basis of many different factors, e.g., termination reactions, chain transfer, competing uncontrolled free radical reactions, thermal production of free radicals, effects of inhibitors and other impurities, dead-end reaction, etc. Theories exist for M_w vs p under different scenarios,[42,43] and a potentially important contribution of ACOMP will be to evaluate such data in the light of the various theoretical predictions to better understand what effects may be operative in real reactions.

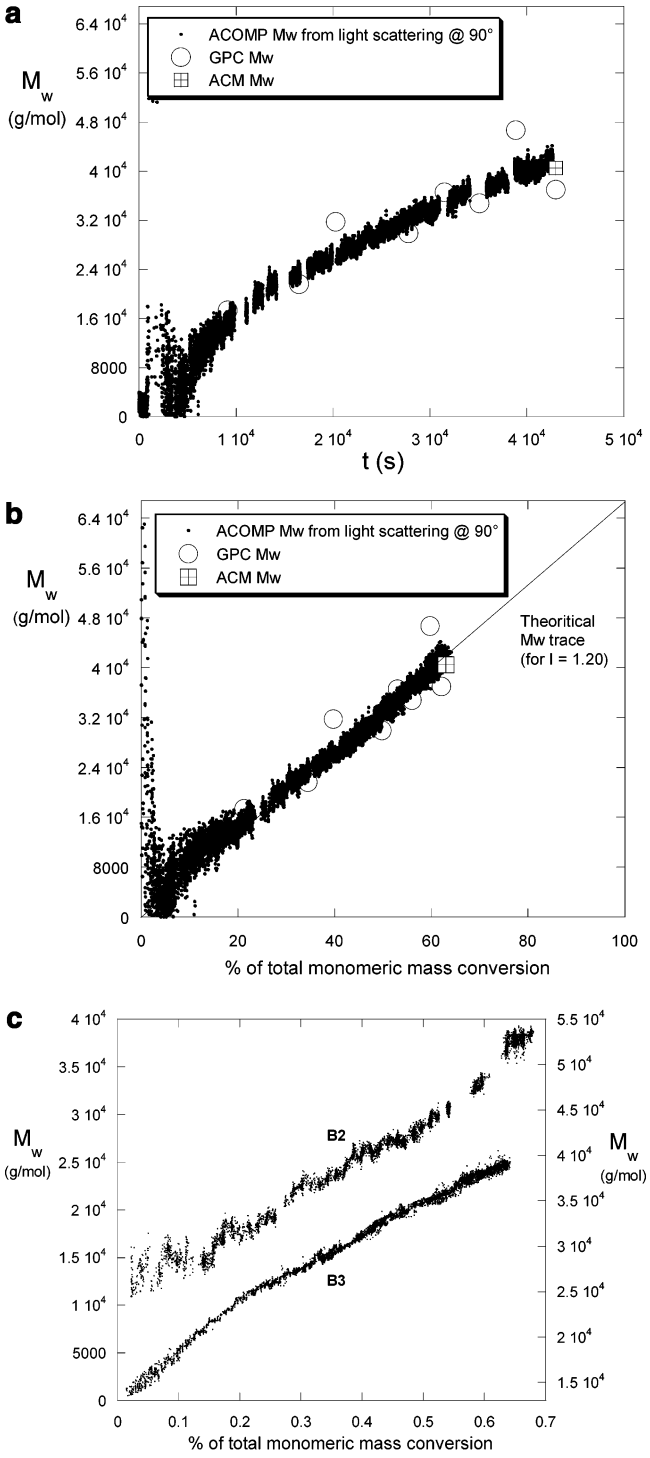

Figure 7. (a) M_w vs time for experiment S3. Hollow circles are GPC results from aliquots withdrawn during the reaction. The square with an inscribed cross is the ACM measurement on the end product. (b) M_w vs % of total monomeric mass conversion for experiment S3. Also shown are GPC points for aliquots withdrawn from the reactor during the polymerization. The square with an inscribed cross is the ACM measurement on the end product. (c) M_w vs % of total monomeric mass conversion for experiments B2 (left-hand axis) and B3 (right-hand axis), showing deviations from linearity.

Table 3. Coefficients from Eq 15 (a_0, a_1, a_2), and Experimental Results on End Products of Various Reactions, As Obtained by ACOMP, ACM, and GPC

				ACOMP			ACM				
expt (st/ba %)	a_0	a_1	a_2	M_w	p	$[\eta]$ final	M_w	10^4A_2	$[\eta]$	GPC M_w	DLS D_H (nm)
B1 (10/90)	3.80×10^{-6}	−0.131	2118	34 600	0.67	32	ND[a]	ND	ND	ND	ND
B2 (20/80)	-1.19×10^{-7}	0.0958	3935	39 500	0.59	45	ND	ND	ND	ND	ND
B3 (30/70)	4.38×10^{-7}	0.3265	191	39 400	0.64	36	ND	ND	ND	ND	ND
S0 (pure ba)	NA[b]	NA	NA	19 500	0.986	11	21 000	7.56	12.23	18 300	7.0
S1 (10/90)	6.736×10^{-8}	−0.0228	1134	35 000	0.863	12.3	33 500	8.65	12.73	36 900	7.5
S2 (30/70)	-6.64×10^{-6}	0.378	262.4	31 600	0.578	15.7	35 000	8.70	15.56	33 000	7.8
S3 (50/50)	3.167×10^{-6}	0.651	−600	40 100	0.638	18	40 500	8.8	16.85	37 000	8.5
S4 (70/30)	2.96×10^{-6}	0.858	−848	49 000[c]	0.635	19.7	ND	ND	18.06	40 600	9.4

[a] ND = no data. [b] NA = not applicable. [c] Using $A_2 = 3 \times 10^{-4}$, close to that of pure PS.

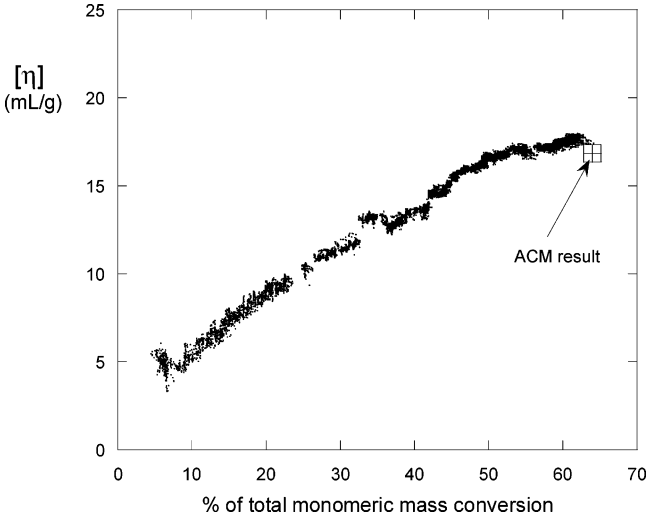

Figure 8. η_r for the same experiment in Figure 7a (S3). The single square point at the end is from an ACM measurement made on the end product.

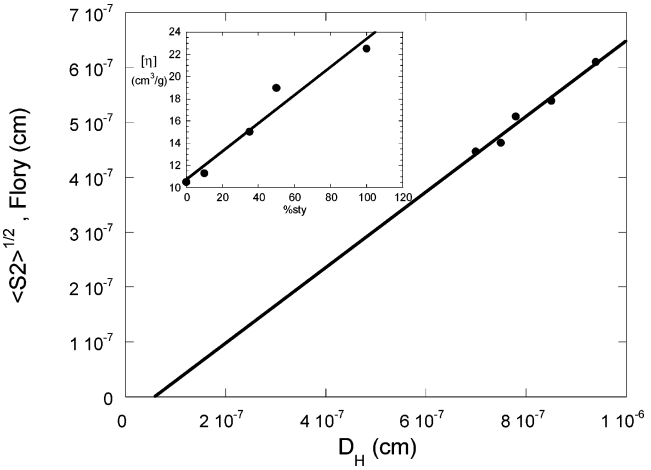

Figure 9. Flory rms radius of gyration from eq 30 from final ACOMP value of $[\eta]_w$ vs D_H, determined by DLS, shown in Table 3. The inset shows the variation of $[\eta]_w$ with styrene composition.

Computation of weight-averaged reduced viscosity $\eta_{r,w}$ does not present the complications of varying $\partial n/\partial c$ and is computed in the usual fashion. Because of the low concentrations of ACOMP (much lower than the overlap concentration) and the small values of $\eta_{r,w}$, it can be assumed to high accuracy that $\eta_{r,w}$ is equal to the intrinsic viscosity $[\eta]_w$. Figure 8 shows the value of $[\eta]_w$ for the same experiment as in Figure 7a, for which M_w is shown.

The values of $[\eta]_w$ varied widely among experiments, even when the final masses were quite close. Table 3 shows final viscosities and masses for the CPR experiments performed in solvent and bulk, with varying proportions of comonomer. The origin of the differences is discussed below.

Combining the ACOMP values of $[\eta]_w$ with D_H from dynamic light scattering (DLS) reveals that there is a strong composition dependence for $[\eta]_w$. Hence, there is no unique Mark−Houwink expression common for copolymers of arbitrary compositions and gradients. It is thus not straightforward to compute the polydispersity index M_w/M_η, as it was for homopolymeric CRP cases.[18]

Copolymer Static and Hydrodynamic Dimensions. Table 3 gives equivalent hydrodynamic diameters D_H, from DLS measurements, where available. Combining M_w and $[\eta]_w$ with the Flory relationship

$$[\eta] = \frac{\Phi_v}{M}[\sqrt{6}\langle S^2\rangle_{Flory}{}^{1/2}]^3 \qquad (30)$$

where $\Phi_v = 2.56 \times 10^{23}$, yields the equivalent root-mean-square Flory radii of gyration, $\langle S^2\rangle_{Flory}{}^{1/2}$, also given in the table. Since polydispersity is low, no corrections for polydispersity are made. Figure 9 shows $\langle S^2\rangle_{Flory}{}^{1/2}$ vs D_H, yielding a good linear correlation with a slope of 0.69. This is remarkably close to the ideal case of a random coil in the nondraining limit, which yields a slope of 0.75.[44] The inset to the figure shows that a fairly linear relationship also exists between D_H and fraction of styrene in the copolymer. The larger value of D_H for PS compared to PBA, even when M_w for each are expressed in terms of degree of polymerization, likely reflects the greater "bead friction" of the styrene ring, compared to PBA, which has no large pendant group.

As a result of the above linear proportionality between D_H and $\langle S^2\rangle_{Flory}{}^{1/2}$, $[\eta]$ is proportional to $D_H{}^3$, as expected. Hence, the viscometer in ACOMP furnishes information essentially equivalent to DLS, at least for low polydispersity (since DLS provides a z-average R_H and the viscometer gives a weight-average viscosity). This suggests that if CRP gradient copolymerization were done with comonomers of widely varying reactivity ratios, so that a strongly changing composition profile was formed, the ACOMP viscosity data in a single experiment could resolve differential friction factors between comonomers.

Conclusions

ACOMP has been applied to CRP gradient copolymerization. It was demonstrated that both the average instantaneous composition $F_{inst,A}$ (which here is termed

the "composition profile") and cumulative mole fraction $F_{cum,pA}$ of each comonomer along the polymer chains can be computed from continuous knowledge of the concentrations of comonomer and copolymer in a model-independent fashion. It is known that different distributions of comonomers yield different macroscopic properties for polymers. Hence, the ability of ACOMP to follow the composition profile should allow for a rich variety of comonomer and initiator schemes to be tried to carefully control the types of profiles actually formed; e.g., comonomers could be fed at differential rates into the reactor to tailor-make desired profiles. Furthermore, the comonomer concentration data allow kinetic models and reactivity ratios to be evaluated.

When the concentration data are combined with static light scattering M_w as a function of time and conversion is obtained, which leads to values that are close to that of the initial stoichiometry. The actual shape of M_w vs p may prove valuable in future analyses to see what type of deviations from the simplest CRP schemes may be occurring, e.g., competing free radical reactions and chain transfer.

Combining concentration data with viscosity data yields $[\eta]_w$. Differences among the viscosity data yield information on the hydrodynamic frictional properties of each comonomer. Aside from the potential practical and fundamental advantages that ACOMP can bring to CRP gradient copolymerization, the method could potentially become a means for studying the fundamental physics of copolymers, such as dimensions and hydrodynamics.

Current efforts include extension of ACOMP to the production of diblock copolymers, polymerization involving comonomers of widely varying reactivity ratio, and to quantify deviations from ideal living behavior. The stage is also set for monitoring branching reactions using polyfunctional comonomers and CRP initiators.[45] ACOMP should also prove useful in evaluating new initiators in CRP.

Acknowledgment. Support from Atofina Elf, NSF CTS 0124006, and NASA NAG-1-02070 and NCC3-946 is gratefully acknowledged.

References and Notes

(1) Matyjaszewski, K., Davis, T. M., Eds. *Handbook of Radical Polymerization*; John Wiley & Sons: Hoboken, 2002.
(2) Hawker, C. J.; Bosman, A. W.; Harth, E. *Chem. Rev.* **2001**, *101*, 3661.
(3) Davis, T. P.; Haddleton, D. M.; Richards, S. N. *J. Macromol. Sci., Rev. Macromol. Chem. Phys.* **1994**, *C34*, 243.
(4) Goto, A.; Fukuda, T. *Macromolecules* **1997**, *30*, 5183.
(5) Georges, M. K.; Veregin, R. P. N.; Kazmeier, P. M.; Hamer, G. K. *Macromolecules* **1993**, *26*, 2987.
(6) Solomon, D. H.; Rizzardo, E.; Cacioli, P. US Patent 4,581,-429.
(7) Matyjaszewski, K.; Ziegler, M. J.; Arehart, S. V.; Greszta, D.; Pakula, T. *J. Phys. Org. Chem.* **2000**, *13*, 775.
(8) Benoit, D.; Hawker, C. J.; Huang, E. E.; Lin, Z.; Russell, T. P. *Macromolecules* **2000**, *33*, 1505.
(9) Annighofer, F.; Gronski, W. *Colloid Polym. Sci.* **1983**, *263*, 15.
(10) Pakula, T.; Matyjaszewski, K. *Macromol. Theory Simul.* **1996**, *5*, 987.
(11) Borner, H. G.; Duran, D.; Matyjaszewski, K.; da Silva, M.; Sheiko, S. S. *Macromolecules* **2002**, *35*, 3387.
(12) Bu, B.; Sen, A. *Macromolecules* **2002**, *35*, 8913.
(13) Aksimentiev, A.; Holyst, R. *J. Chem. Phys.* **1999**, *111*, 2329.
(14) Pickett, G. T. *J. Chem. Phys.* **2003**, *118*, 3898.
(15) Shull, K. R. *Macromolecules* **2002**, *35*, 8631.
(16) Catalgil-Giz, H.; Giz, A.; Alb, A. M.; Oncul A. K.; Reed, W. F. *Macromolecules* **2002**, *35*, 6557.
(17) Stockmayer, W. H. *J. Chem. Phys.* **1945**, *13*, 199.
(18) Mayo, F. R.; Lewis, F. M. *J. Am. Chem. Soc.* **1944**, *66*, 1594.
(19) Grimaldi, S.; LeMoigne, F.; Finet, J. P.; Tordo, P.; Nicol, P.; Plechit, P. Patent W096/24620, 1996.
(20) Benoit, D.; Grimaldi, S.; Robin, S.; Finet, J. P.; Tordo, P.; Gnanou, Y. *J. Am. Chem. Soc.* **2000**, *122*, 5929.
(21) Couturier, J. L.; Guerret, O. Patent FR 2,812,639, 2000.
(22) LeMercier, C.; Lutz, J. F.; Marque, S.; Lemoigne, F.; Tordo, P.; LaCroix-Desmazes, P.; Boutevin, B.; Couturier, J. L.; Guerret, O.; Martschke, R.; Sobek, J.; Fischer, H. *ACS Symp. Ser.* **2000**, *768*, 108.
(23) Guerret, O.; Couturier, J. L.; Le Mercier, C. WO 200248159, 2002.
(24) Florenzano, F. H.; Strelitzki, R.; Reed, W. F. *Macromolecules* **1998**, *31*, 7226.
(25) Chauvin, F.; Alb, A. M.; Bertin, D.; Tordo, P.; Reed, W. F. *Macromol. Chem. Phys.* **2000**, *203*, 2029.
(26) Norwood, D. P.; Reed, W. F. *Int. J. Polym. Anal. Charact.* **1997**, *4*, 99.
(27) Berne, B.; Pecora, R. *Dynamic Light Scattering*; John Wiley & Sons: New York, 1976.
(28) Brousseau, J.-L.; Giz, H. Ç.; Reed, W. F. *J. Appl. Polym. Sci.* **2000**, *77*, 3259.
(29) Walling, C. *J. Am. Chem. Soc.* **1988**, *110*, 6846.
(30) Daikh, B. E.; Finke, R. G. *J. Am. Chem. Soc.* **1992**, *114*, 2938.
(31) Fischer, H. *Macromolecules* **1997**, *30*, 5666.
(32) Fischer, H. *Chem. Rev.* **2001**, *101*, 3581.
(33) Walling, C. H.; Briggs, E. R. *J. Am. Chem. Soc.* **1945**, *67*, 1774.
(34) Kelen, T.; Tudos, F.; Turksanyi, B.; Kennedy, J. P. *J. Polym. Sci., Polym. Chem. Ed.* **1977**, *15*, 3047.
(35) Zammit, M. D.; Davis, T. P.; Willett, G. D.; O'Driscoll, K. F. *J. Polym. Sci., Part A: Polym. Chem.* **1997**, *35*, 2311.
(36) Arehart, S. V.; Matyjaszewski, K. *Macromolecules* **1999**, *32*, 2221.
(37) Habibi, A.; Farahani, E. V.; Semsarzadeh, M. A.; Sadughiani, K. *Macromol. Theory Simul.* **2003**, *12*, 184.
(38) Rodriguez, F. *Principles of Polymer Systems*, 3rd ed.; Hemisphere Pub. Corp.: Bristol, PA, 1989.
(39) Odian, G. *Principles of Polymerization*, 3rd ed.; John Wiley & Sons: New York, 1991.
(40) Stockmayer, W. H.; Moore, L.D.; Fixman, M.; Epstein, B. N. *J. Polym. Sci.* **1955**, *16*, 517.
(41) Bushuk, W.; Benoit, H. *Can. J. Chem.* **1958**, *36*, 1616.
(42) Souaille, M.; Fischer, H. *Macromolecules* **2002**, *35*, 248.
(43) Souaille, M.; Fischer, H. *Macromolecules* **2001**, *34*, 2830.
(44) Yamakawa, H. *Modern Theory of Polymer Solutions*; Harper & Row: New York, 1971.
(45) Guerret, O.; Couturier, J. L.; Vuillemin, B.; Lutz, J. F.; Le Mercier, C.; Robin, S. FR 99/06329, Elf Atochem, 1999.

MA035589B